Xiaoqiang Li[1], Minai Zhang[1, 2,*], Xiaojian Xia[1], Ting Cao[1], Liang Liang[1], Huiyun Li[3]

[1]Guangdong Key Laboratory for Advanced Metallic Materials Fabrication and Forming, South China University of Technology, Guangzhou, China

[2]Chemical Engineering and Materials Science, University of California, Irvine, United State of America

[3]Dongguan hyperpowder Co. Ltd., Dongguan, China

*zhang.ma@hotmail.com

Corrosion behavior of WC–10 wt % Ni₃Al composite in acidic media

The room temperature corrosion behavior of WC–10 wt % Ni₃Al composite and WC–8 wt % Co hardmetal in various acidic solutions (1 M H₂SO₄, 1 M HCl and 1 M HNO₃) were compared and investigated utilizing immersion test, electrochemical measurement and surface analytical techniques. The results show that in H₂SO₄ solution WC–10Ni₃Al composite has a nobler free corrosion potential, lower corrosion current density (I_{corr}) values and intrinsically better corrosion resistance than WC–8Co. Notably, pseudopassivity was observed in the polarization curves of WC–10Ni₃Al in both HCl and H₂SO₄ solutions. In addition, although WC–10Ni₃Al is corroded much faster in HNO₃ solution than in the other two mediums, it exhibits a superior corrosion resistance compared to WC–8Co. The corrosion mechanism of WC–10Ni₃Al composites is dominated by Ni dissolution.

Keywords: WC–10Ni₃Al composite, intermetallics, corrosion, polarization, pseudopassivity.

INTRODUCTION

WC–Co based hardmetals, which possess high hardness and strength, have been widely used in engineering components, such as cutting tools, drill tips and seal rings [1–3]. However, their applications have been limited due to their poor corrosion resistance [4, 5]. A considerable amount of research has been focused on the corrosion behavior of WC hardmetal [6–9]. S. Hochstrasser [5] found that the composition of the binder phase was the main factor affecting the corrosion resistance of cemented carbide. The corrosion properties of WC–Co in acidic and neutral electrolytes were controlled by the dissolution of Co binder [4, 5]. Several attempts have been made to overcome the corrosion susceptibility of WC–Co based hardmetals [6–15]. One method involved the introduction of other carbide phases (VC, Cr₃C₂, TaC, TiC and ZrC) [11, 12, 16, 17] which led to improvements in passivation resistance of the WC–Co alloys. Another method involved replacing the Co binder with other corrosion-resistant metallic binders such as Ni, Ni–Cr, Ni–Cr–Mo [13–15, 18]. Bozzini et al. confirmed that binders containing Ni would improve the corrosion resistance of cemented carbides in neutral and acidic media [19, 20].

Intermetallic compounds such as Ni₃Al have unique high temperature properties and excellent corrosion/oxidation resistance [21, 22]. Developments in the

processing of intermetallic alloys over the last few decades have resulted in their adoption in a variety of industries [21, 23]. In these alloys, the third element is used to enhance the mechanical properties. Recently, to get excellent performance at elevated temperatures and under corroding environments, intermetallic compounds such as Ni_3Al and Fe_3Al have been used as the binder phase to replace Co in WC–Co system [24, 25]. It has been confirmed that Ni_3Al has sufficient wettability with WC grains, which can facilitate the formation of dense bulk WC–Ni_3Al [23]. The WC–40 vol % Ni_3Al composite have good mechanical properties comparable to WC–Co [26]. Liang et al. [2] confirmed that the wear resistance of WC–10 wt % Ni_3Al composite is superior to that of WC–8 wt % Co cemented carbides. Although the research on intermetallic compounds as binders in WC materials is still scarce, composites such as WC–Ni_3Al are expected to be highly competitive as hard materials.

In our previous study [27, 28], the WC–10 wt % Ni_3Al with plate-like triangular prismatic WC gains were successfully fabricated by mechanical alloying plus spark plasma sintering, and showed excellent mechanical properties and oxidation resistance. To further explore the potential of this material, the present research focuses on its corrosion behavior in various acidic media at room temperature.

MATERIAL AND METHODS

In the experiments, WC–10Ni_3Al[*] composites with plate-like triangular prismatic WC grains were fabricated by preparing WC–Ni_3Al mixed powders by wet milling and subsequent sintering with Dr. Sinter Model SPS-825 Spark Plasma Sintering System (Sumitomo Coal Mining Co. Ltd., Japan), as described in Reference [27]. It is important to note that the Ni_3Al powders were mechanically alloyed with a composition of Ni–10.50Al–10.90Fe–8.12Cr–0.89Zr–0.21B, with the primary phase being Ni_3Al, as identified by X-ray diffraction (XRD). Boron is added as the key trace addition since it improves the grain boundary cohesive strength and room temperature ductility [29]. The other alloying additions include Fe, Cr, and Zr give the Ni_3Al powder higher strength [29].

Immersion corrosion testing was conducted according to ASTMG31-12a. 1 M HCl, 1 M HNO_3 and 1 M H_2SO_4 water solutions were used as the static corrosion media for the immersion test at room temperature. Before the test, samples were machined into plates with the size of 20×50×1.6 mm and all the surface were polished with successively finer polishes (3 μm → 1.5 μm → 0.5 μm), then the surface area and weight were measured on an electronic balance with a precision of ±0.1 mg. The polished samples were immersed into the acid solution and protected in a sealed environment. After immersion for 100 h, the samples were removed, cleaned with alcohol in an ultrasonic water bath for 20 s and dried at room temperature for further characterization. The samples were reweighed for determination of specific mass loss. The corrosion rate was calculated by the formula

$$\upsilon_{corr} = \Delta G/ST, \qquad (1)$$

where υ_{corr} is the corrosion rate, G is the weight loss (g), S is the surface area of the sample (m^2), and T is the immersion time (h).

The electrolytes used in the experiments were 1 M HCl and 1 M H_2SO_4. A three-electrode-cell setup with a potentiostat unit (CHI660D, ChenHua Co., China) was used for the electrochemical experiments. The tested specimen, saturated

---

[*] Hereinafter, the composition is given in wt %.

calomel electrode (SCE) and Pt sheet were respectively used as working electrode, reference electrode and auxiliary electrode. Prior to the experiments, samples were coated with insulating paint except a working area of 1 cm^2 to be exposed to the electrolyte. The open circuit potentials (E_{oc}) tests were conducted for 1 h after the samples were immersed in the electrolyte. Potentiodynamic polarization measurements were performed by polarizing samples from –0.6 to 1.2 V at a scan rate of 2 mV/s. Then, chronoamperometric measurements were performed for 2 h on the polarized surface of the samples, in which the applied potential was selected from the corresponding polarization curve. All the experiments were repeated at least three times with good repeatability. The phase constitutions of the samples after electrochemical measurements were identified by an X-ray photoelectron spectroscopy (XPS) using a spectrometer with a nonmonochromatized X-ray source (Al$K\alpha$). Energy-dispersive spectroscopy (EDS) coupled with scanning electron microscopy (SEM) (Nova Nano 430, FEI, USA) were used to observe the microstructure and morphology of the specimens.

RESULTS AND DISCUSSION

Immersion test

The characteristics of the raw materials used to fabricate WC–10Ni$_3$Al composites are shown in Table 1. Commercial bulk materail WC–8Co (Changcheng YG8, Zigong cemented carbide Co., China) was used for comparison. The nominal compositions of the as-prepared and as-received cemented carbides are presented in Table 2. SEM micrographs of the as-consolidated WC–10Ni$_3$Al and WC–8Co before test are shown in Fig. 1. Plate-like triangular prismatic WC grains (grey phase) were found in the WC–10Ni$_3$Al materials (see Fig. 1, *a*), while the WC–8Co displayed a more equiaxed microstructure (see Fig. 1, *b*). The dark phases are Ni$_3$Al and Co, respectively. The results indicate that the average grain size of the two composites is similar at approximately 2 μm, even though the morphologies of the grains are quite different.

Table 1. Characterization of the starting powders used to fabricate WC–10Ni$_3$Al composites

Powder	Purity, %	Average particle size, μm
WC	≥ 99.9	0.6
Ni	≥ 99.5	2.6
Al	≥ 99.5	90
Fe	≥ 99.5	6.0
Cr	≥ 99.0	75
Zr	≥ 99.9	75
B	≥ 99.0	75

Table 2. The nominal compositions of the WC–10Ni$_3$Al and WC–8Co, wt %

	WC	Ni	Al	Fe	Cr	Zr	B	Co
WC–10Ni$_3$Al	Bal.	6.94	1.05	1.09	0.812	0.089	0.021	–
WC–8Co	Bal.	–	–	–	–	–	–	8
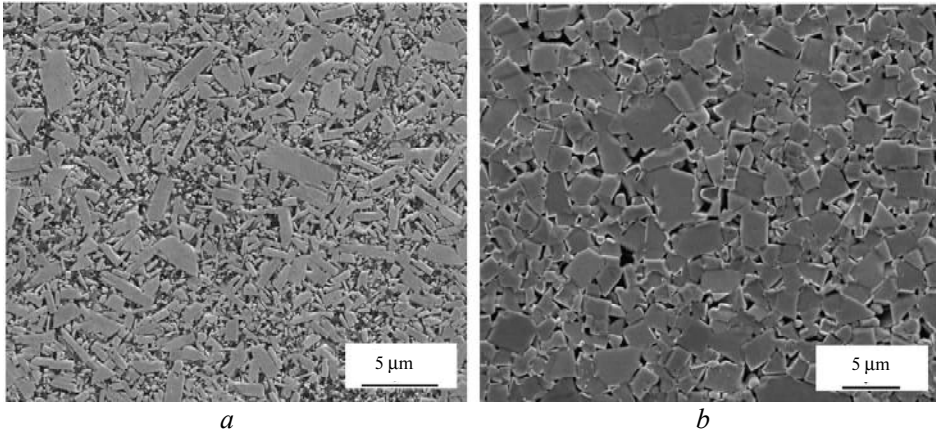
Fig. 1. SEM micrographs of SPS-consolidated WC–10Ni$_3$Al (*a*) and WC–8Co (*b*) before corrosion test.

Figure 2 shows the average corrosion rates of WC–10Ni$_3$Al and WC–8Co in 1 M acid solution at room temperature over 100 h. In H$_2$SO$_4$ solutions, the average corrosion rate of WC–8 Co is twice as high as that of WC–10Ni$_3$Al. In HCl medium the difference in corrosion rate between the two materials is negligible. Both WC–10Ni$_3$Al and WC–8Co have the highest corrosion rate in HNO$_3$ solution, which is much higher than their values in H$_2$SO$_4$ and HCl solutions. The Ni$_3$Al bonded WC show excellent resistance to nitric and sulfuric [24], similar results have been observed previously in Ni–WC materials [18]. Ni plays a very important role in the corrosion process.
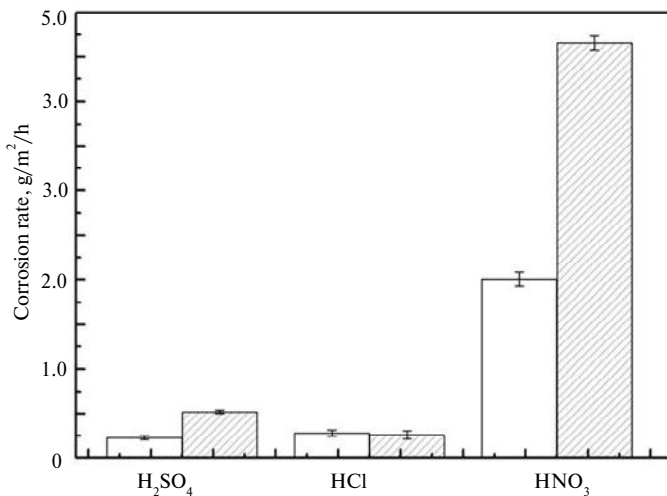
Fig. 2. Average corrosion rates of WC–10Ni$_3$Al (□) and WC–8Co (▪) in 1 M acid solution at room temperature over 100 h.

In the three kinds of acid solutions, the reaction of Co in the WC–8Co depends on the following formula:

$$Co \rightarrow Co^{2+} + 2e^{-},$$
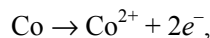
which can be confirmed from the orange color of the solution (Co^{2+}). In HNO$_3$, particularly, a deep yellow precipitant (WO$_3$) is formed and adsorbed on the sur-

face of the samples. This is due to HNO_3 being a strong oxidizing and corrosive inorganic acid. The reaction of WC depends on the following formula [9, 17]:

$$WC + 5H_2O \rightarrow WO_3 + CO_2 + 10H^+ + 10e^-.$$
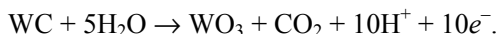
For WC–10 Ni_3Al in HNO_3, Cr is not soluble in HNO_3, which is apt to form passivation film on the surface, thus its corrosion rate is significantly smaller than that of WC–8 Co, so that we do not have any additional discussion in electrochemical measurements section.

In HCl, the reaction depends on the following formulae [30]:

$$Ni + 2H^+ \rightarrow Ni^{2+} + H_2;$$

$$Al + 3H^+ \rightarrow Al^{3+} + H_2;$$

$$Fe + 2H^+ \rightarrow Fe^{2+} + H_2;$$

$$Cr + 2H^+ \rightarrow Cr^{2+} + H_2;$$

$$Co + 2H^+ \rightarrow Co^{2+} + H_2.$$
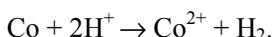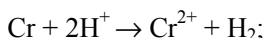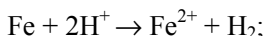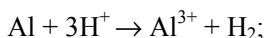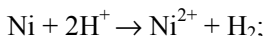
Since the standard electric potentials of Al (–1.66 V), Fe (–0.45 V) and Cr (–0.93 V) in WC–10 Ni_3Al are lower than that of Co (–0.28 V), WC–10 Ni_3Al is likely to have a reaction with HCl. As a result, its corrosion rate is slightly higher than that of WC–8 Co.

Figure 3 shows the corrosion morphology of WC–10Ni_3Al and WC–8Co after immersion in 1 M H_2SO_4 for 100 h, and the EDS spectra from the selected areas. Serious corrosion damage and cracks were observed on the surface of WC–8 Co in Fig. 3, *b*. In contrast, the corrosion damage in the WC–10 Ni_3Al is noticeably less, with no apparent pores and cracks observed on its surface. But there exists some localized corrosion damage, which may result from the non-uniform microstructures. It is further illustrated that WC–10 Ni_3Al exhibits better corrosion resistance in H_2SO_4. From the EDS analysis results of the selected areas shown in Figs. 3, *c* and *d*, the corrosion surface still contains Al, Ni and Fe for WC–10 Ni_3Al and Co for WC–8Co. These findings imply that these elements do not completely dissolve in the solution under the present corrosion conditions. Besides the composition of binder phase, WC grain size and volume fraction of binder also may influence the corrosion resistance of WC materials [10]. This study only focuses on the effect of binder type, others features will not be discussed.

a	*b*
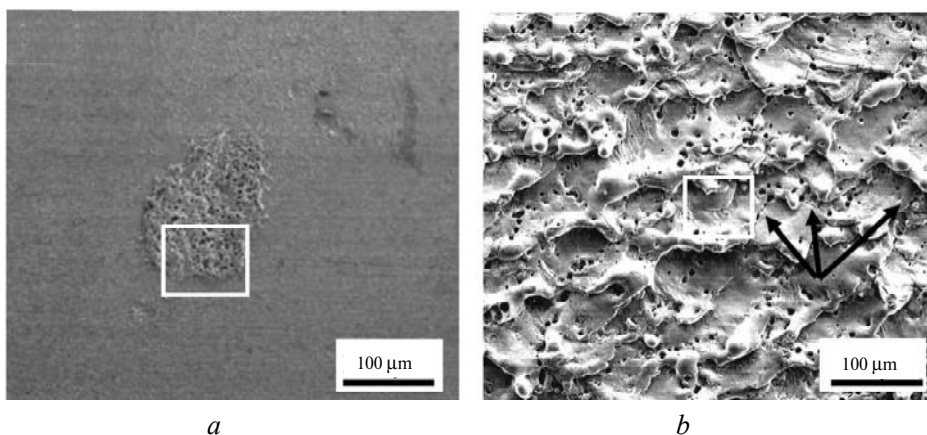
Fig. 3. Corrosion morphology of WC–10Ni_3Al (*a*) and WC–8Co (*b*) after immersion in 1 M H_2SO_4 for 10 h; (*c*) and (*d*) show EDS from the selected areas in (*a*) and (*b*), respectively.
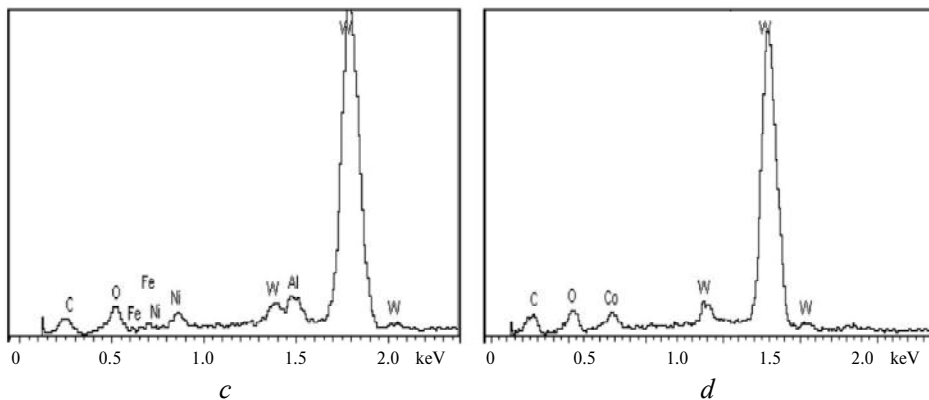
Fig. 3. (Contd.)

Electrochemical measurements

The open circuit potential (OCP) curves of WC–10 Ni₃Al and WC–8 Co in HCl and H₂SO₄ are presented in Fig. 4. The potential curves in both solutions are stable and basically smooth with increasing immersion time, implying the two materials are not susceptible to pitting in both of these solutions. The results are similar with those for WC–VC–Co, WC–FeAl–B and WC–TiC–Ni [13, 16, 25]. This illustrates that WC itself has an intrinsic corrosion resistance. The differences between the materials result from the different binder phases. The E_{oc} value of WC–8Co in HCl somewhat decreases in the first 40 min, indicated that some corrosion happens on the surface. After 40 min, the E_{oc} value increases, which indicates the appearance of passivation behavior. In H₂SO₄, both the E_{oc} values of WC–10Ni₃Al and WC–8Co are relatively constant. The OCP value for the WC–10Ni₃Al is nobler than that of the WC–8 Co in both H₂SO₄ and HCl, which indicates that with the addition of the alternative binder Ni₃Al the corrosion resistance of WC material is improved.
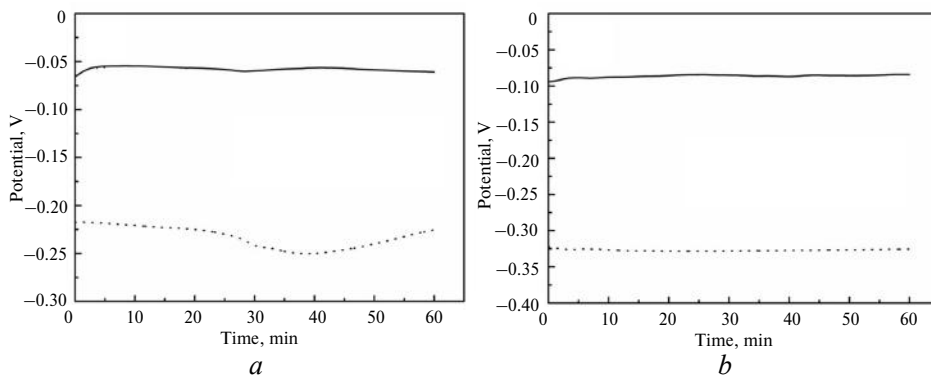
Fig. 4. OCP curves of WC–10Ni₃Al (—) and WC–8Co (····) in 1 M HCl (*a*) and 1 M H₂SO₄ (*b*) at room temperature.

Figure 5 shows the potentiodynamic polarization curves for WC–10Ni₃Al and WC–8Co in HCl and H₂SO₄. Both WC–10Ni₃Al and WC–8Co show pseudopassivation behavior marked by a small decrease in current density at higher potentials. The corrosion parameters of the two materials in HCl and H₂SO₄ are summarized in Table 3. In HCl, the anodic Tafel constant of the two materials are constant throughout the test. The anodic Tafel constant of WC–8Co is suddenly increased at about 0 V, which is in agreement with the report on WC–10Co in reference [31].

The onset of pseudopassive behavior of the two materials is roughly at the same potential. The value of free corrosion potential represents a thermodynamic characteristic for a given metal-electrolyte system. According to Table 3, WC–10Ni$_3$Al has a nobler free corrosion potential than WC–8Co, which means that the corrosion of the later initiates earlier. However, WC–10Co has a slightly lower corrosion current density (I_{corr}) value. The I_{corr} was determined by extrapolating the linear Tafel segments of the anode and cathode polarization curves. The value of I_{corr} reflects the corrosion rate more accurately than E_{corr}, due to the fact that the corrosion current value represents the corrosion kinetics of the material [17]. Under the combined effects of an immersion test, OCP and potentiodynamic polarization curves, the corrosion resistance of WC–10Ni$_3$Al is slightly worse than WC–8Co in HCl. In H$_2$SO$_4$, the pseudopassivity of WC–8Co is in agreement with literature. The anode critical passivation current density of WC–10Ni$_3$Al is close to 10 μA/cm^2 and its pseudopassivation range is greater than that of WC–8Co. It is obvious that the onset of pseudopassivation is earlier for WC–10Ni$_3$Al and the decrement of current density is larger. The E_{corr} and I_{corr} values for WC–10Ni$_3$Al are –0.112 V and 8.0 μA/cm^2, and –0.324 V and 51.0 μA/cm^2 for WC–8Co. WC–10Ni$_3$Al has both nobler E_{corr} and significantly lower I_{corr} values. Consequently, it possesses stronger corrosion resistance in H$_2$SO$_4$ than WC–8Co, which is different than the behavior in HCl.
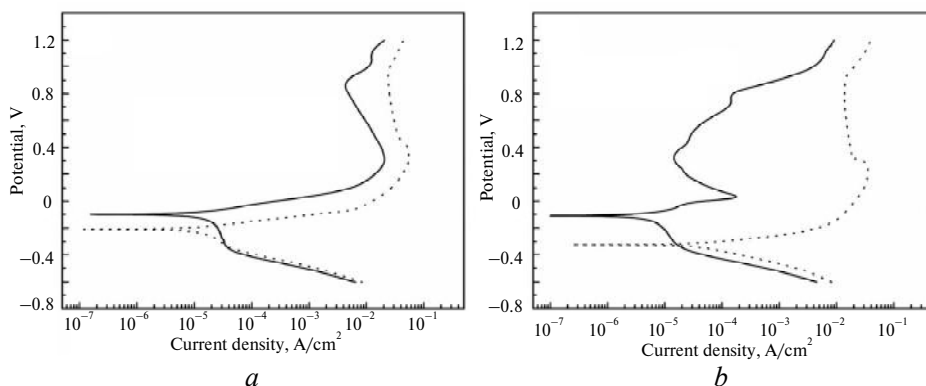
Fig. 5. Potentiodynamic polarization curves of WC–10Ni$_3$Al (—) and WC–8Co (····) in 1 M HCl (*a*) and 1 M H$_2$SO$_4$ (*b*) at room temperature.

Table 3. The corrosion parameters of WC–10Ni$_3$Al and WC–8 in HCl and H$_2$SO$_4$ from potentiodynamic polarization curves

Composition, wt %	HCl		H$_2$SO$_4$	
	E_{corr}, V	I_{corr}, μA/cm^2	E_{corr}, V	I_{corr}, μA/cm^2
WC–10 Ni$_3$Al	–0.099	13.2	–0.112	8.0
WC–8 Co	–0.208	12.4	–0.324	51.0

The variations in current density during chronoamperometric testing are shown in Fig. 6. The potentials used for chronoamperometric testing were selected from the positions in the anodic polarization curves where the current densities do not change with potential. Tests were thus done at 0.7 and 0.5 V (SCE) for WC–10 Ni$_3$Al, 0.8 and 0.6 V (SCE) for WC–8 Co in HCl and H$_2$SO$_4$, respectively. The chronoamperometric curves of the two materials possess a similar trend of decay in current density to a steady value. These results indicate that corrosion and sponta-

neous passivation occurs alongside the gradual densification of a passive film. WC–10Ni₃Al possesses the lowest steady state value in both solutions. WC–8Co, however, has a sharp reduction in current density, which occurs during the initial stage in both the solutions. This is because a thin passive film forms on the surface and the oxidation kinetics decayed by logarithmic mode, which agrees well with literatures [4, 5]. The decay and subsequent stabilization in current density further suggests that passivation has been developed.
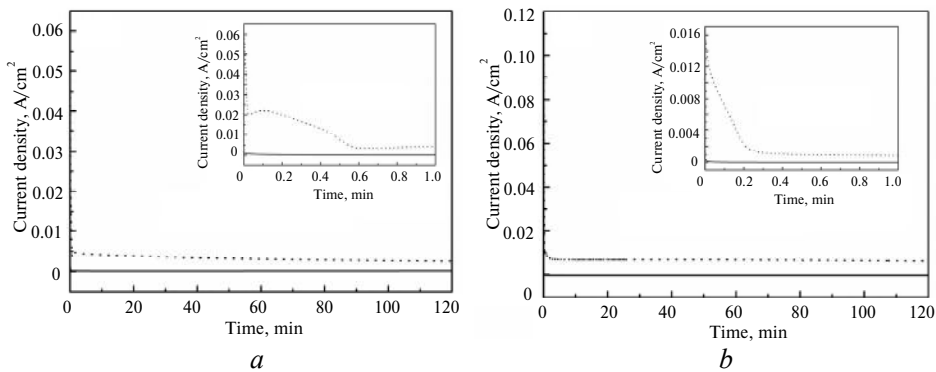
Fig. 6. Comparison of the chronoamperometry curves of WC–10Ni₃Al (—) and WC–8 Co (····) in 1 M HCl (*a*) and 1 M H₂SO₄ (*b*).

XPS analysis after corrosion

The XPS spectra of the specimens after the potentiodynamic polarization tests reveal the chemical composition of the corrosion products, as shown in Figs. 7 and 8, respectively. It is easy to identify a serious corrosion occurred from the W 4f and O 1s spectra in the whole XPS spectra (see Fig. 7, *a* and Fig. 8, *a* in both acids. In the WC–8Co specimens, fitted high-resolution W 4f and Co 2p spectra shown in the Figs. 7, *b* and *c*. There were three $4f_{7/2}$–$4f_{5/2}$ spin-split doublets in W 4f spectra in both acids, which can be confirmed that WC, WO_3 and WO_2. This imply thin oxide films formed on the surface in both acids. There were two $2p_{3/2}$–$2p_{1/2}$ spin-split doublets in Co 2p spectrum corresponding to $Co(OH)_2$ and Co_3O_4 in HCl while three main peaks in H_2SO_4 corresponding to CoO, $Co(OH)_x(SO_4)_y$ and Co_3O_4 [32], this indicates that micro-galvanic coupling occurred in HCl while no significant micro-galvanic coupling in H_2SO_4. The Co preferentially react with acids and then WC slowly eroding.

Figures 8, *b*–*d* shows the fitted high-resolution W 4f, Ni 2p and Al 2p spectra when Ni₃Al as the binder. Because of the low content of alloying element of Fe and Cr, the peaks were unreliable and can be ignored. Same to the WC–Co, there were three peaks in W 4f corresponding to WC, WO_3 and WO_2. Similarly, it can be seen from Fig. 8, *c* that there were two spin-split doublets corresponding to $Ni(OH)_2$ and Ni_2O_3 in HCl while three peaks in H_2SO_4 corresponding to NiO, $Ni(OH)_x(SO_4)_y$ and Ni_2O_3. Meanwhile, there were two $2p_{3/2}$–$2p_{1/2}$ spin-split doublets in Al 2p spectrum corresponding to AlO_x and $Al_2O_3/Al(OH)_3$ [33]. It is noted that the intensity of W 4f in WC–8Co is higher than WC–10 Ni₃Al, this imply more W reacting the corrosion process, this means that the oxide films formed by the Ni₃Al can protect the specimen, therefore, the WC–10Ni₃Al have a better corrosion resistance in H_2SO_4. In addition, micro-galvanic coupling also occurred in HCl because of the exists of the Ni, and the Al promote the coupling. This result in that the corrosion resistance of WC–Ni₃Al is slightly worse than WC–Co. From the

analysis of the product, Ni as the main element in Ni₃Al alloy plays an important role in the corrosion process and its corrosion mechanisms are dominated by Ni dissolution.
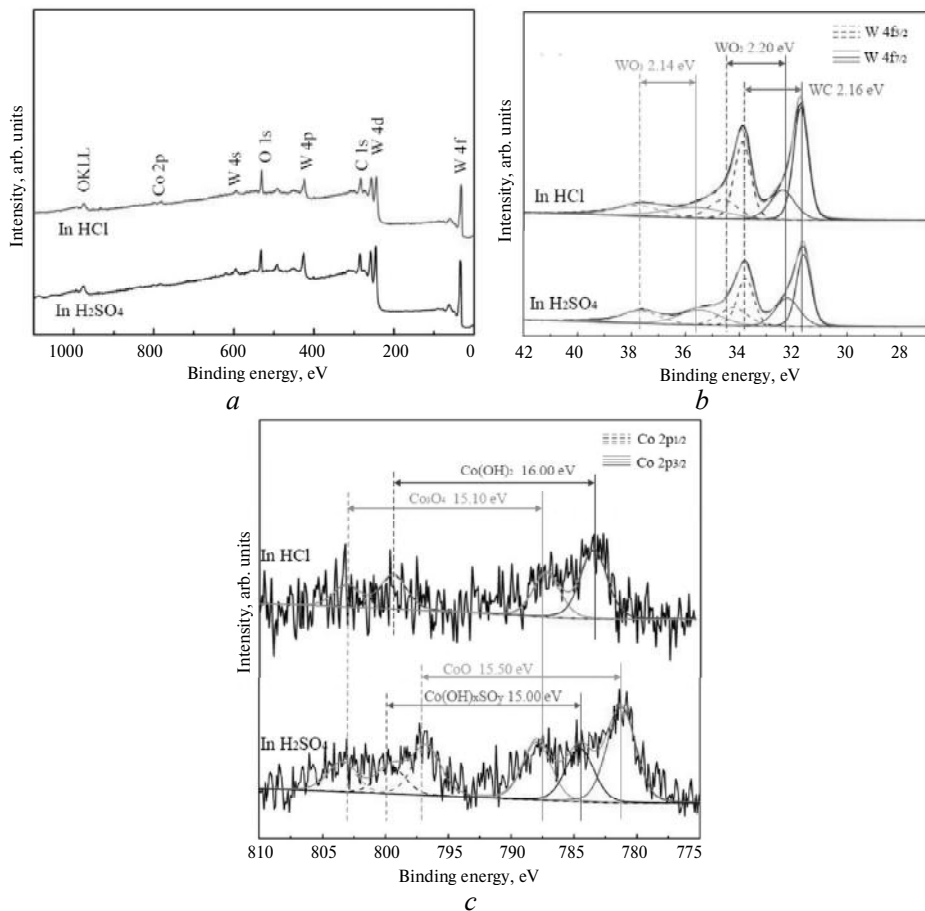
Fig. 7. Whole XPS spectra (*a*) and high-resolution W 4f (*b*) and Co 2p (*c*) XPS spectra obtained from surfaces of WC–8Co after corrosion (experimental spectra: black lines; fitted spectra: gray lines).
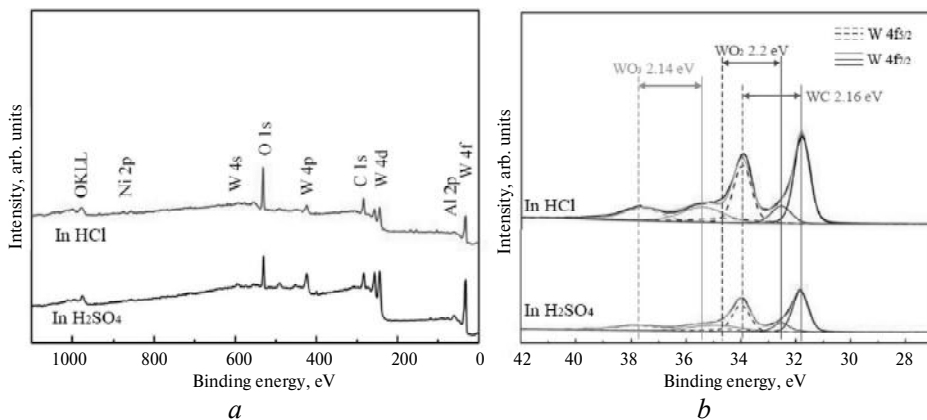
Fig. 8. Whole XPS spectra (*a*) and high-resolution W 4f (*b*), Ni 2p (*c*) and Al 2p (*d*) XPS spectra obtained from surfaces of WC–10Ni₃Al after corrosion (experimental spectra: black lines; fitted spectra: gray lines).
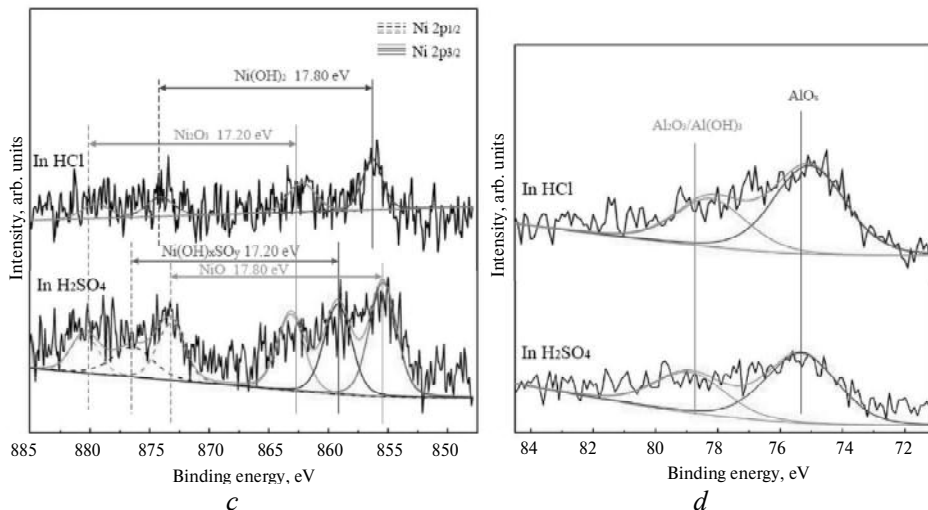
Fig. 8. (Contd.)

CONCLUSIONS

In this study, the corrosion behavior of WC–10Ni₃Al has been investigated and compared to that of WC–8Co in 1 M HCl and 1 M H₂SO₄ at room temperature. The results of open circuit potential and corrosion current densities showed that the WC–10Ni₃Al was not susceptible to pitting corrosion in H₂SO₄ solution. All the samples showed pseudopassive behavior, and combining with the immersion results, the corrosion resistance of WC–10Ni₃Al is slightly worse than that of the WC–8Co in HCl. In HNO₃, however, the immersion results indicate a better corrosion resistance for WC–10Ni₃Al. Moreover, the corrosion mechanism of the WC–10Ni₃Al composites is dominated by Ni dissolution.

FUNDING

Порівняно корозійну поведінку при кімнатній температурі композита WC–10 % (за масою) Ni₃Al та твердого металевого сплаву WC–8 % (за масою) Co у різних кислотних розчинах (1 M H₂SO₄, 1 M HCl та 1 M HNO₃), що була досліджена за допомогою методу занурення, електрохімічного вимірювання та поверхневих аналітичних методів. Результати показали, що в розчині H₂SO₄ композит WC–10Ni₃Al має високий потенціал вільної корозії, менші значення щільності корозійного струму (I_corr) та кращу стійкість до корозії, ніж WC–8Co. Помічено, що псевдопасивність спостерігалася в поляризаційних кривих WC–10Ni₃Al як в розчині HCl, так і в H₂SO₄. Крім того, хоча WC–10Ni₃Al кородує в розчині HNO₃ набагато швидше, ніж у двох інших середовищах, він виявляє кращу стійкість до корозії порівняно з WC–8Co. У механізмі корозії композитів WC–10Ni₃Al переважає розчинення Ni.

Ключові слова*: композит WC–10Ni₃Al, інтерметаліди, корозія, поляризація, псевдопасивність.*

Проведено сравнение коррозионного поведения при комнатной температуре композита WC–10 % (по массе) Ni₃Al и твердого металлического сплава WC– (по массе) Co в различных кислотных растворах (1 M H_2SO_4, 1 M HCl и 1 M HNO_3), исследованное с помощью метода погружения, электрохимического измерения и поверхностных аналитических методов. Результаты показали, что в растворе H_2SO_4 композит WC–10Ni₃Al имеет высокий потенциал свободной коррозии, меньшие значения плотности коррозионного тока (I_{corr}) и лучшую устойчивость к коррозии, чем WC–8Co. Замечено, что псевдопасивность наблюдалась в поляризационных кривых WC–10Ni₃Al как в растворе HCl, так и в H_2SO_4. Кроме того, хотя WC–10Ni₃Al корродирует в растворе HNO_3 гораздо быстрее, чем в двух других средах, он обнаруживает лучшую устойчивость к коррозии по сравнению с WC–8Co. В механизме коррозии композитов WC–10Ni₃Al преобладает растворения Ni.

Ключевые слова: композит WC–10Ni₃Al, интерметаллиды, коррозия, поляризация, псевдопассивность.

1. Fang Z.Z., Wang X., Ryu T., Hwang K.S., Sohn H.Y. Synthesis, sintering, and mechanical properties of nanocrystalline cemented tungsten carbide – A review. *Int. J. Refract. Met. Hard Mater.* 2009. Vol. 27, no. 2. P. 288–299.
2. Liang L., Liu X., Li X.-q., Li Y.-Y. Wear mechanisms of WC–10Ni₃Al carbide tool in dry turning of Ti₆Al₄V. *Int. J. Refract. Met. Hard Mater.* 2015. Vol. 48. P. 272–285.
3. Wang X., Hwang K.S., Koopman M., Fang Z.Z., Zhang L. Mechanical properties and wear resistance of functionally graded WC–Co. *Int. J. Refract. Met. Hard Mater.* 2013. Vol. 36. P. 46–51.
4. Engqvist H., Beste U., Axén N. The influence of pH on sliding wear of WC-based materials. *Int. J. Refract. Met. Hard Mater.* 2000. Vol. 18, no. 2. P. 103–109.
5. Hochstrasser S., Mueller Y., Latkoczy C., Virtanen S., Schmutz P. Analytical characterization of the corrosion mechanisms of WC–Co by electrochemical methods and inductively coupled plasma mass spectroscopy, *Corros. Sci.* 2007. Vol. 49, no. 4. P. 2002–2020.
6. Exner H.E. Physical and chemical nature of cemented carbides. *Int. Metals Rev.* 1979. Vol. 24, no. 1. P. 149–173.
7. Human A.M., Exner H.E., Electrochemical behaviour of tungsten-carbide hardmetals. *Mater. Sci. Eng. A.* 1996. Vol. 209, no. 1. P. 180–191.
8. Human A.M., Roebuck B., Exner H.E. Electrochemical polarisation and corrosion behaviour of cobalt and Co(W,C) alloys in 1 N sulphuric acid *Mater. Sci. and Eng. A.* 1998. Vol. 241, no. 1. P. 202–210.
9. Sutthiruangwong S., Mori G. Corrosion properties of Co-based cemented carbides in acidic solutions. *Int. J. Refract. Met. Hard Mater.* 2003. Vol. 21, no. 3. P. 135–145.
10. Kellner F.J.J., Hildebrand H., Virtanen S. Effect of WC grain size on the corrosion behavior of WC–Co based hardmetals in alkaline solutions. *Int. J. Refract. Met. Hard Mater.* 2009. Vol. 27, no. 4. P. 806–812.
11. Lin N., Wu C.H., He Y.H., Zhang D.F. Effect of Mo and Co additions on the microstructure and properties of WC–TiC–Ni cemented carbides. *Int. J. Refract. Met. Hard Mater.* 2012. Vol. 30, no. 1. P. 107–113.
12. Wan W., Xiong J., Yang M., Guo Z., Dong G., Yi C. Effects of Cr₃C₂ addition on the corrosion behavior of Ti(C, N)-based cermets. *Int. J. Refract. Met. Hard Mater.* 2012. Vol. 31. P. 179–186.
13. Zhang Q., Lin N., He Y. Effects of Mo additions on the corrosion behavior of WC–TiC–Ni hardmetals in acidic solutions. *Int. J. Refract. Met. Hard Mater.* 2013. Vol. 38. P. 15–25.
14. Su W., Sun Y., Liu J., Feng J., Ruan J. Effects of Ni on the microstructures and properties of WC–6Co cemented carbides fabricated by WC–6(Co, Ni) composite powders. *Ceram. Int.* 2015. Vol. 41, no. 2, Part B. P. 3169–3177.
15. Andrews N., Giourntas L., Galloway A.M., Pearson A. Erosion–corrosion behaviour of zirconia, WC–6Co, WC–6Ni and UNS S31600. *Int. J. Refract. Met. Hard Mater.*, 2015. Vol. 48. P. 229–237.
16. Konadu D.S., van der Merwe J., Potgieter J.H., Potgieter-Vermaak S., Machio C.N. The corrosion behaviour of WC–VC–Co hardmetals in acidic media. *Corros. Sci.* 2010. Vol. 52, no. 9. P. 3118–3125.

17. Lin N., He Y., Wu C., Liu S., Xiao X., Jiang Y. Influence of TiC additions on the corrosion behaviour of WC–Co hardmetals in alkaline solution. *Int. J. Refract. Met. Hard Mater.* 2014. Vol. 46. P. 52–57.

18. Gao L.X., Zhou T., Zhang D.Q., Lee K.Y. Microstructure and anodic dissolution mechanism of brazed WC–Ni composite coatings. *Corros. Eng. Sci. and Tech.* 2014. Vol. 49, no. 3. P. 204–208.

19. Bozzini B., Serra M., Fanigliulo A., Bogan F. Corrosion behaviour of WC–Co based hard-metalin neutral chloride and acid sulphate media. *Mater. Corros.* 2002. Vol. 53, no. 5. P. 328–334.

20. Bozzini B., De Gaudenzi G.P., Mele C. Electrochemical behaviour of alloy CoW0·013C0·001 in acidic sulphate solutions. *Corros. Eng. Sci. Techn.* 2005. Vol. 40, no. 2. P. 149–157.

21. Sikka V.K., Deevi S.C., Viswanathan S., Swindeman R.W., Santella M.L. Advances in processing of Ni_3Al-based intermetallics and applications. *Intermetallics*. 2000. Vol. 8, no. 9. P. 1329–1337.

22. Wagle S., Kaneno Y., Nishimura R., Takasugi T. Evaluation of the wear properties of dual two-phase Ni_3Al/Ni_3V intermetallic alloys. *Tribo. Int.* 2013. Vol. 66. P. 234–240.

23. Sikka V.K., Mavity J.T., Anderson K. Processing of nickel aluminides and their industrial applications. High Temperature Aluminides and Intermetallics. Oxford: Elsevier, 1992. P. 712–721.

24. Tiegs T.N., Alexander K.B., Plucknett K.P., Menchhofer P.A., Becher P.F., Waters S.B. Ceramic composites with a ductile Ni_3Al binder phase. *Mater. Sci. Eng. A.* 1996. Vol. 209, no. 1. P. 243–247.

25. Habibi Rad M., Ahmadian M., Golozar M.A. Investigation of the corrosion behavior of WC–FeAl–B composites in aqueous media. *Int. J. Refract. Met. Hard Mater.* 2012. Vol. 35. P. 62–69.

26. Long J., Zhang Z., Xu T., Lu B. Microstructure, mechanical properties and fracture behavior of WC–40 vol % Ni_3Al composites with various carbon contents. *Int. J. Refract. Met. Hard Mater.* 2013. Vol. 40. P. 2–7.

27. Li X., Chen J., Zheng D., Qu S., Xiao Z. Preparation and mechanical properties of WC–10 Ni_3Al cemented carbides with plate-like triangular prismatic WC grains. *J. Alloys Compd.* 2012. Vol. 544. P. 134–140.

28. Li X., Zhang M., Zheng D., Cao T., Chen J., and Qu S., The oxidation behavior of the WC–10 wt % Ni_3Al composite fabricated by spark plasma sintering, *J. Alloys Compd.*, 2015. Vol. 629. P. 148–154.

29. Nazarian Samani M., Shokuhfar A., Kamali A.R., Hadi M. Production of a nanocrystalline Ni_3Al-based alloy using mechanical alloying. *J. Alloys Compd.* 2010. Vol. 500, no. 1. P. 30–33.

30. Bard Allen J., Faulkner Larry R. Electrochemical Methods: Fundamentals and Applications. Texas: Wiley, 2000.

31. Sutthiruangwong S., Mori G., Kösters R. Passivity and pseudopassivity of cemented carbides. *Int. J. Refract. Met. Hard Mater.* 2005. Vol. 23, no. 2. P. 129–136.

32. Mao Q., Yang Q., Xiong W., Li S., Zhang M., Ruan L. Corrosion behavior of Ni_3Al-bonded TiC-based cermets in H_2SO_4 and NaOH solutions. *Ceram. Int.* 2018. Vol. 44. P. 13303–13312.

33. Xu Y., Yoshikawa H., Jang J.H. Characterization of surface structure evolution in Ni_3Al foil catalysts by hard X-ray photoelectron spectroscopy. *J. Phys. Chem. C.* 2010. Vol. 114. P. 6047–6053.